ACS Catalysis

Research Article

pubs.acs.org/acscatalysis

Alkene Epoxidation Catalysts [Ru(pdc)(tpy)] and [Ru(pdc)(pybox)] Revisited: Revealing a Unique Ru^{IV}=O Structure from a Dimethyl Sulfoxide Coordinating Complex

Ying Wang,[¶,□,†] Lele Duan,[□,‡] Lei Wang,[‡] Hong Chen,[§,⊥] Junliang Sun,[§] Licheng Sun,[*,‡,∥] and Mårten S. G. Ahlquist[*,†]

[†]Division of Theoretical Chemistry and Biology, School of Biotechnology, KTH Royal Institute of Technology, 10691 Stockholm, Sweden

[‡]Department of Chemistry, School of Chemical Science and Engineering, KTH Royal Institute of Technology, SE-100 44 Stockholm, Sweden

[§]Berzelii Center EXSELENT on Porous Materials and Department of Materials and Environmental Chemistry, Stockholm University, SE-106 91 Stockholm, Sweden

[⊥]Faculty of Material Science and Chemistry, China University of Geosciences, 430074, Wuhan, China

[∥]State Key Lab of Fine Chemicals, DUT-KTH Joint Education and Research Center on Molecular Devices, Dalian University of Technology (DUT), 116024 Dalian, China

Supporting Information

ABSTRACT: The X-ray crystal structure of a dimethyl sulfoxide (DMSO) coordinating complex [Ru^{II}(κ^2-pdc)(tpy)(DMSO)] (H_2pdc = 2,6-pyridyl dicarboxylic acid and tpy = 2,2′:6′,2″-terpyridine) led to the discovery of a unique Ru^{IV}=O configuration for the Ru-pybox (pybox = pyridine-bis(oxazoline) ligands) epoxidation catalyst by theoretical calculations. On the basis of this structure, a detailed theoretical study was conducted on the alkene epoxidation reaction using ruthenium-based epoxidation catalysts. It was found that the process of H_2O_2 coordination proceeded via an associative path in which one carboxylate detached. The following H_2O-elimination step was found to be facilitated by the detached carboxylate group. The resulting Ru^{IV}=O rearranges to the species *trans*-**2a**-oxo, in which one carboxylate group is situated over the tpy ring; the *trans*-**2a**-oxo was found to have the lowest activation free energies toward alkene epoxidation. These results demonstrated the importance of the hemilabile properties of the pdc^{2-} ligand for the Ru-pdc alkene epoxidation catalysts.

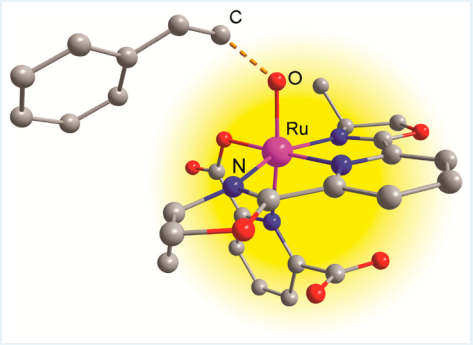

KEYWORDS: *epoxidation, ruthenium, DFT, hemilabile, oxidation, mechanism*

INTRODUCTION

Asymmetric epoxidation of alkenes is a central reaction in organic synthesis, especially for drug synthesis because it can potentially generate two chiral centers in one step. During the past few decades, large progress has been made in the development of epoxidation catalysts. Some of the most well-known catalysts are the Sharpless–Katsuki Ti tartrate complexes[1] and the Katsuki–Jacobsen Mn-salen complexes.[2,3] However, those catalysts require the use of non-atom-economic reagents as the oxidant, such as alkyl hydroperoxides and hypochlorite. In recent years, great efforts have been dedicated to epoxidation reactions using hydrogen peroxide as the terminal oxidant because hydrogen peroxide has high atom economy and its only byproduct is water.[4]

Ruthenium-based epoxidation catalysts have received much attention because of the well-developed Ru chemistry and the easy access of various redox states of Ru complexes.[5−26] In particular, Nishiyama et al. reported the first use of [Ru(pdc)(tpy)] (**1**; H_2pdc = 2,6-pyridyl dicarboxylic acid; tpy = 2,2′:6′,2″-terpyridine; Figure 1) as an alkene-epoxidation catalyst in the presence of non-atom-economic oxidants such as $PhI(OAc)_2$, O_2/^{t}BuCHO, and ^{t}BuOOH.[27] Later on, Beller and co-workers developed a series of catalysts of [Ru(pdc)(pybox)] (pybox = pyridine-bis(oxazoline) ligands; complex **2**; Figure 1) that use hydrogen peroxide as the oxidant, with high activity and selectivity toward asymmetric epoxidation of alkenes.[28−32] The anionic ligand pdc^{2-} is essential to suppress the decomposition of hydrogen peroxide and to improve the efficiency of the Ru-pdc/H_2O_2 system toward alkene epoxidation. It has also been used in water oxidation catalysts in which the π-donating pdc^{2-} ligand makes the high valent states accessible at lower potentials.[33−35]

Received: March 9, 2015
Revised: May 20, 2015
Published: May 21, 2015

DOI: 10.1021/acscatal.5b00496
ACS Catal. 2015, 5, 3966−3972

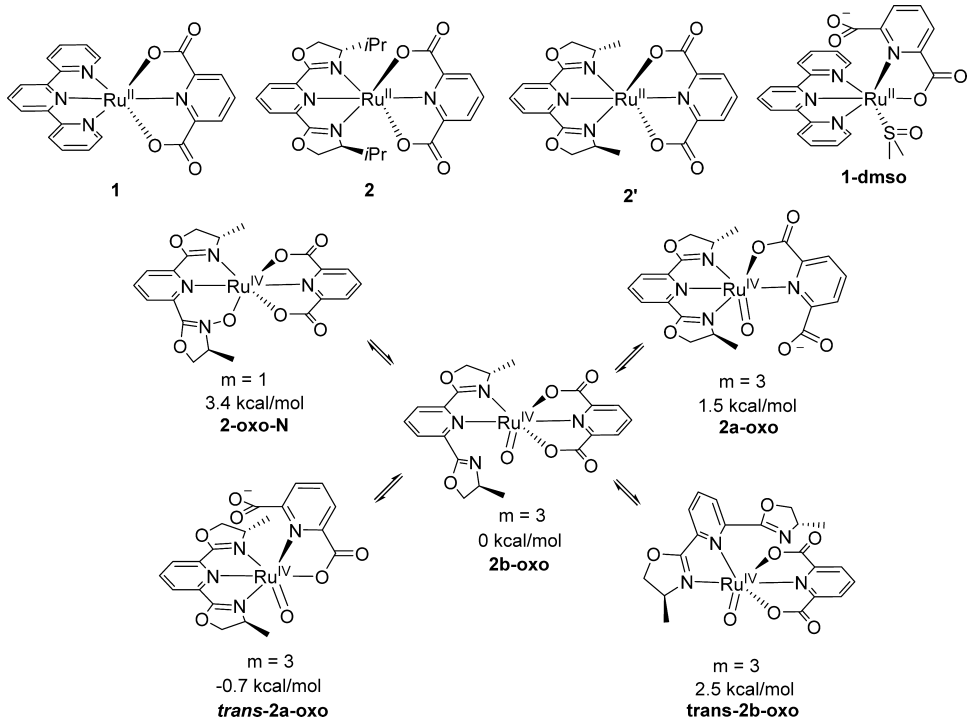

Figure 1. Structures of complexes **1**, **2**, **2′**, **1**-DMSO, **2a**-oxo, **2b**-oxo, *trans*-**2a**-oxo, *trans*-**2b**-oxo, and *trans*-**2a**-oxo, as well as free energy differences of oxo species The spin multiplicity (m) of each oxo complex is labeled.

For the epoxidation reaction, it was proposed that the corresponding Ru^{IV}═O species, [Ru^{IV}(pdc)(κ^2-pybox)(O)] (**2b**-oxo; Figure 1), is the active catalyst on the basis of density function theory (DFT) calculations.[29] Unfortunately, limited experimental results were obtained to identify the geometric structure of the active Ru^{IV}═O because of the intrinsic difficulty in isolating the reactive/unstable, high valent state Ru^{IV}═O species. This also hampers the understanding and the development of the Ru-pdc alkene epoxidation catalysts. Herein, we report the crystal structure of a novel DMSO-coordinated Ru-pdc complex [Ru^{II}(κ^2-pdc)(tpy)(DMSO)] (**1**-DMSO; DMSO = dimethyl sulfoxide, Figure 1) in which one carboxylate has been detached. On the basis of this finding, we conducted theoretical studies on the function of the hemilabile pdc ligand on the reactivity. We found the *trans*-**2a**-oxo species (Figure 1) to be the most probable intermediate for C−O bond formation in the alkene epoxidation catalyzed by the Ru-pdc-pybox catalyst.

MATERIALS AND METHODS

Experimental Section. Complexes **1** and **2** were prepared according to the literature methods.[27,36] All other chemicals are commercially available. The ^{1}H NMR spectra were recorded using a 500 MHz Bruker Advance spectrometer. Mass spectrometry measurements were performed on a LCQ Advantage Max (Finnigan) mass spectrometry. All of the electronic absorption spectra were measured with a PerkinElmer Lambda 750 UV−vis spectrophotometer.

Synthesis of Complex 1-DMSO. To a dark solid of complex **1** (30 mg) was added 5 mL of dimethyl sulfoxide. The mixture was sonicated for 5 min and then stirred for another 10 min at room temperature. During this period, a yellow precipitate was formed, which was eventually filtered out, washed with ethyl ether/methanol (v/v = 10:1), and dried under vacuum overnight. The target product was obtained as a yellow solid (yield: 15 mg, 43%). ^{1}H NMR (500 MHz, D_2O): δ = 8.36−8.39 (m, 4H), 8.30 (d, 2H), 8.17 (m, 2H), 8.10 (t, 2H), 7.96 (t, 1H), 7.57 (t, 2H), 7.13 (d, 1H), 2.77 (s, 6H). MS (ESI): m/z^+ = 578.93 ([M + H]$^+$ calcd: 579.03) and 600.80 ([M + Na]$^+$; calcd: 601.01). Found: C 50.18, H 3.68, N 9.65. Calcd for $C_{24}H_{20}N_4O_5RuS$: C 49.91, H 3.49, N 9.70%.

Single-Crystal X-ray Diffraction. Single crystals were obtained by a solvent evaporation process of a mixed DMSO/H_2O solution of **1**. Single-crystal X-ray diffraction data were collected from a red blocklike crystal on an Xcalibur diffractometer at 298 K using a Mo X-ray radiation source (λ = 0.71073 Å). Data reduction was performed using the CrysAlisPro program.[37] The structure was solved by a direct method. All the non-hydrogen atoms were located directly from difference Fourier maps. All the hydrogen atoms were located directly in the calculated position on the basis of their geometry. Final structure refinements were performed with the SHELX program[38,39] by minimizing the sum of the squared deviation of F^2 using a full matrix technique.

Computational Studies. All density functional theory (DFT) calculations were carried out with the Jaguar 7.6 program package by Schrödinger LLC. For geometry optimizations, solvation energy, and frequency calculations, Becke's three-parameter hybrid functional and the LYP correlation functional (B3LYP)[40,41] were used with the LACVP** core potential and basis set; single-point energy corrections were performed with the M06[42] functional using the LACV3P**++ basis set which, as suggested by Martin,[43] was augmented with two f-polarization functions on Ru. Frequency calculations were performed on the optimized geometries to verify that the geometries correspond to minima or first-order saddle points (transition states) on the potential energy surface (PES). The Gibbs free energies were defined using the following equation $G = E$(M06/LACV3P**++ 2f on Ru) + G_{solv} + ZPE + H_{298} − TS_{298} + 1.9 (concentration

DOI: 10.1021/acscatal.5b00496
ACS Catal. 2015, 5, 3966−3972

correction to the free energy of solvation from $M(g)$ to $M(aq)$). On the basis of the gas-phase-optimized structures, the effect of solvent was evaluated by single-point calculations using the Poisson−Boltzmann reactive field implemented in Jaguar 7.6 (PBF)[44] in *tert*-butyl alcohol.

RESULTS AND DISCUSSION

Dissolving the dark red solid of complex **1** in DMSO resulted in a light yellow solution from which a yellow precipitate was formed in a few minutes and was isolated and characterized as complex **1**-DMSO in a zwitterionic form. The crystal structure of **1**-DMSO was resolved and is depicted in Figure 2. In the

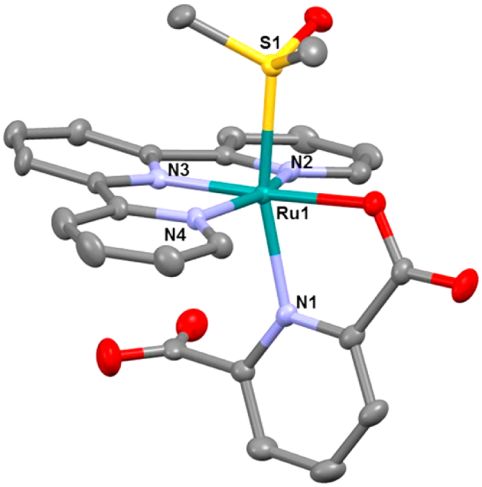

Figure 2. Crystal structure of **1**-DMSO with thermal ellipsoids at 30% probability. Hydrogen atoms are omitted for clarity.

structure, the tpy ligand is tridentately bound to the Ru cation, the pdc ligand bidentately coordinates to the Ru cation though the N and O atoms, and the DMSO ligand binds through the S atom. The DMSO ligand is trans to the N atom of the pdc ligand; one of the carboxylate groups is pendant and is situated close to the tpy ring, as a result of which the central pyridine motif of the terpyridine ligand was clearly bent toward the DMSO ligand. Its ^{1}H NMR and COSY spectra (Figure S1) are in good agreement with the crystal structure resolved from single-crystal X-ray diffraction. Three resonance peaks at 8.17 (including one proton from tpy), 7.96, and 7.13 ppm were assigned to the pdc^{2-} ligand, and the remaining peaks in the aromatic region, to the tpy ligand. The resonance peak of the coordinated DMSO ligand was observed at 2.77 ppm, with a contaminant peak (2.69 ppm) of free DMSO nearby. Regarding the well-known asymmetric alkene epoxidation catalyst **2**, the ligand exchange between methanol and carboxylate ligands has been observed previously by the Beller group;[29] however, the proposed steric structure of the resulting product (the incoming methanol ligand is proposed cis to the pendant free carboxylate) is questionable in consideration of the crystal structure of **1**-DMSO.

Ligand exchange processes are among the most important elementary steps of a catalytic cycle and may influence the catalytic activity, substrate selectivity and the longevity of a catalytic reaction. In particular, a ligand exchange step is required to form the active Ru^{IV}=O at the Ru-pdc catalysts, and therefore, how Ru^{IV}=O is formed is of interest. However, the inherent difficulties of studying the reaction between a Ru-pdc catalyst with H_2O_2, due to decomposition of H_2O_2 and highly reactive intermediates, prevent chemists from obtaining much useful information from experiments. Instead, studying the interaction of a Ru-pdc catalyst with DMSO is easier and more straightforward and may shed light on the ligation of, for example, H_2O_2 with complexes **1** and **2**. We therefore studied the kinetics of reactions of complexes **1** and **2** with DMSO (Figure 3; **2**-DMSO = [Ru(κ^2-pdc)(pybox)(DMSO)]) by

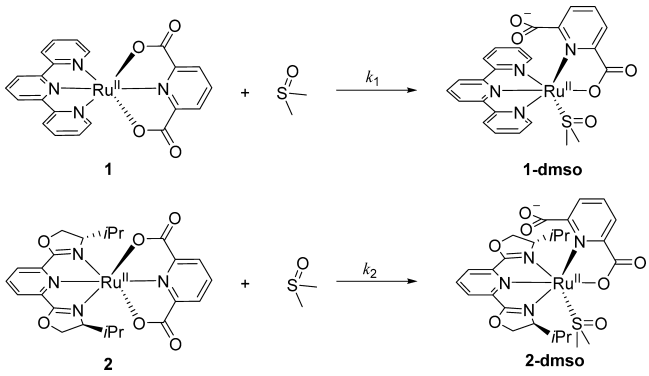

Figure 3. Reaction schemes of **1** (or **2**) + DMSO → **1**-DMSO (or **2**-DMSO).

means of UV−vis spectroscopy (see Figure S2 for the UV−vis spectra of complexes **1** and **2**). Kinetic measurements, by using the initial reaction rate method (Figures S3−S12), reveal a rate law of first order in [Ru] ([**1**] or [**2**]) and first order in [DMSO], which is rate = k[Ru][DMSO], with $k_1 = 1.95 \times 10^{-2}$ M^{-1} s^{-1} for complex **1** and $k_2 = 2.4 \times 10^{-3}$ M^{-1} s^{-1} for complex **2** at room temperature, indicating an associative ligand exchange mechanism. The slow kinetics of **2** are most likely due to two reasons: (1) the electron-deficient Ru cation (caused by the poor electron-donating pybox ligand in which two-electron-negative oxygen atoms are present) strengthens the Ru−$O_{carboxylate}$ bonds and slows down the ligand exchange kinetics; (2) the steric bulkiness of isopropyl groups hinders the incoming DMSO ligand and thereby reduces the ligand exchange rate.

To provide a detailed interpretation for DMSO substitution, DFT calculations were performed to locate the transition states of the ligand substitution reaction. Two transition states were found (Figures 4 and S13): ts-*cis*-**1**-DMSO corresponds to the substitution of the carboxylate ligand close to the incoming DMSO ligand, yielding an intermediate *cis*-**1**-DMSO; ts-**1**-DMSO is the replacement of one carboxylate with the other one, through which *cis*-**1**-DMSO is transformed to **1**-DMSO. The free energy barriers are calculated to be at 15.9 and 15.7 kcal/mol for these two steps, respectively.

The unique structure of **1**-DMSO is reminiscent of the structure of the proposed active Ru^{IV}=O species of the Ru-pdc-pybox asymmetric alkene epoxidation catalysts. We therefore wonder if they share a similar feature, that one of the carboxylates is replaced by the incoming ligand, a DMSO/oxo ligand? To answer this question, we carried out DFT calculations on the structures of Ru=O species. The free energy of five possible active species is first presented, including four Ru^{IV}=O species—**2a**-oxo, **2b**-oxo, *trans*-**2a**-oxo and *trans*-**2b**-oxo—together with a ligand oxidized species (an N oxide) **2**-oxo-N (Figure 1; see their optimized structures in Figure S14). Note that two isopropyl groups of **2** were replaced by two methyl groups **2′** in the DFT calculations.

DOI: 10.1021/acscatal.5b00496
ACS Catal. 2015, 5, 3966−3972

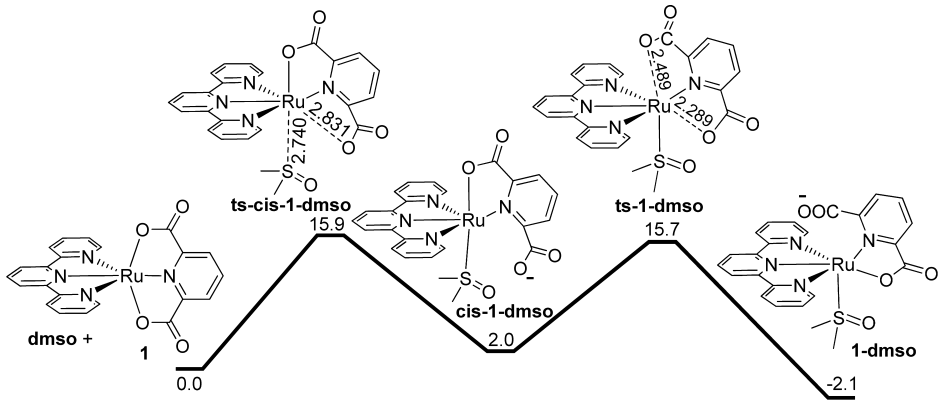

Figure 4. Reaction diagram of the DMSO-substitution reaction. The relative Gibbs free energies are given in kcal/mol, and the bond lengths are given in Å.

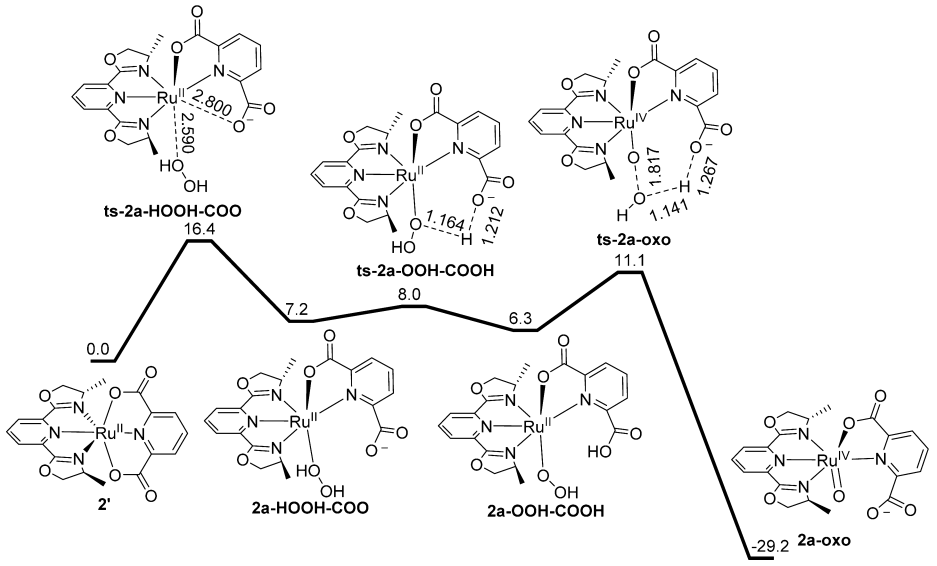

Figure 5. Reaction diagram of formation of **2a**-oxo via H_2O_2 with complex **2′**. The relative Gibbs free energies are given in kcal/mol, and the bond lengths are given in Å.

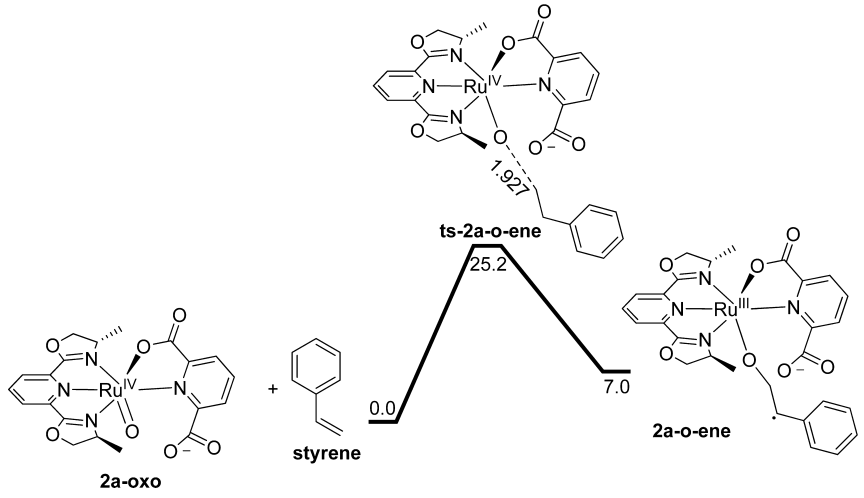

Figure 6. Reaction diagram of epoxidation of styrene using **2a**-oxo. The relative Gibbs free energies are given in kcal/mol, and the bond lengths are given in Å.

Among these five species, complex *trans*-**2a**-oxo is calculated to have the lowest free energy. The other conformations are all slightly higher in free energy, yet all low enough to be possible candidate reactive species. Complex **2**-oxo-N is not considered as a reactive species because it has to be transformed to a Ru═O species to react with an alkene, and it was not further

DOI: 10.1021/acscatal.5b00496
ACS Catal. 2015, 5, 3966−3972

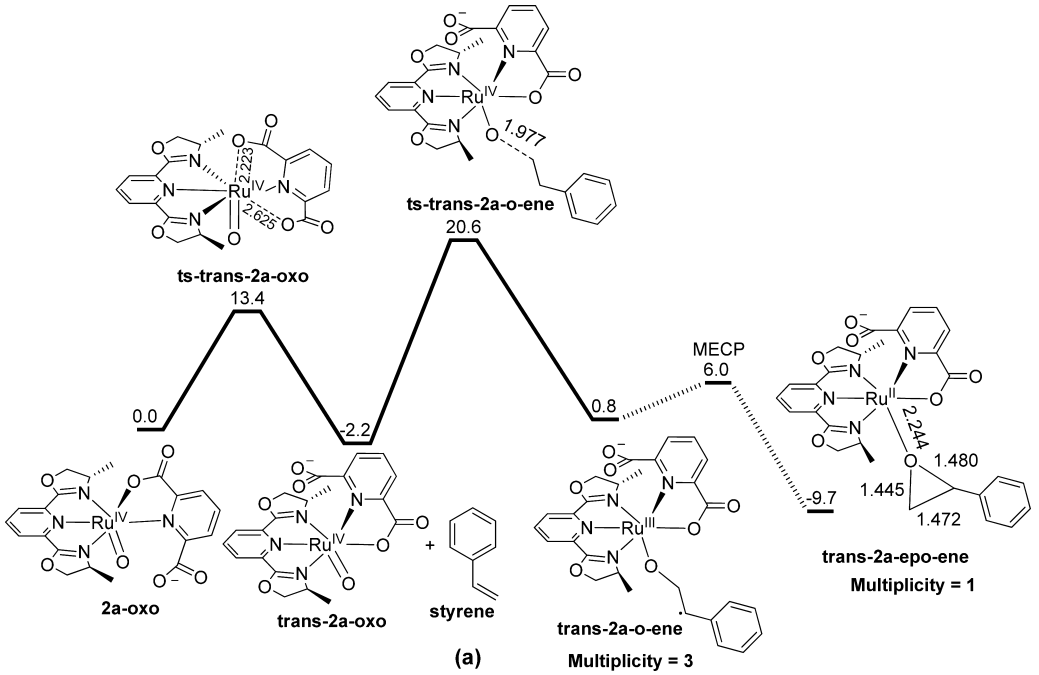

Figure 7. Epoxidation of styrene using *trans*-**2a**-oxo. The relative Gibbs free energies are given in kcal/mol, and the bond lengths are given in Å.

investigated. On the basis of these values, we cannot identify whether **2a**-oxo, **2b**-oxo, *trans*-**2a**-oxo, or *trans*-**2b**-oxo is the active species. Therefore, we calculated their reaction energy barriers toward the C−O bond formation for the alkene epoxidation reaction.

First, the formation of the relatively stable epoxidation catalysts **2a**-oxo and **2b**-oxo were examined. For **2a**-oxo, as inspired by the DMSO-substitution reaction (Figure S13a), we explored the ligation of H_2O_2 to the complex **2′** with the involvement of carboxylate ligand dissociation (Figure 5; optimized structures in Figure S15). Upon the approach of HOOH to complex **2′**, the carboxylate ligand close to the incoming HOOH dissociates, and **2a**-HOOH−COO is formed with an activation barrier of 16.4 kcal/mol via the transition state ts-**2a**-HOOH−COO. Then a proton of the attached HOOH is transferred to the oxygen site of the dissociated carboxylate ligand. This proton movement is facile and proceeds with a low free energy barrier of 0.8 kcal/mol via ts-**2a**-OOH−COOH and leads to the formation of complex **2a**-OOH−COOH. The formation of the potential catalyst **2a**-oxo is accompanied by the dissociation of water and is exergonic once the free energy barrier ts-**2a**-oxo is overcome (11.1 kcal/mol). The direct formation of **2b**-oxo from the reaction of **2′** and HOOH is disfavored with a free energy barrier of 29.9 kcal/mol (Figure S16).

The free energy barriers for styrene reacting with the species **2b**-oxo and *trans*-**2b**-oxo where a nitrogen ligand has dissociated, are calculated at 27.8 and 29.6 kcal/mol, respectively (Figures S17 and S18), indicating that these two reactions would be slow at room temperature. In contrast, the energy barriers for the species with the detached carboxylate, **2a**-oxo and *trans*-**2a**-oxo, are lower. Therefore, the following discussion will focus on these two species to understand how Ru-pdc complexes catalyze alkene epoxidation.

The free energy barrier of direct reaction of catalyst **2a**-oxo with styrene is calculated as 25.2 kcal/mol relative to **2a**-oxo via ts-**2a**-o-ene (Figure 6), indicating that this direct reaction between **2a**-oxo and styrene to complete the epoxidation is slow at room temperature. Once the potential catalyst **2a**-oxo is formed, another possible pathway that includes the transition to *trans*-**2a**-oxo by overcoming ts-*trans*-**2a**-oxo (13.4 kcal/mol) before reacting with styrene is considered (Figure 7). This reaction is exergonic by 2.2 kcal/mol, and *trans*-**2a**-oxo is actually the Ru^{IV}-oxo species with the lowest free energy. Therefore, all reactions with styrene should be related to this species. This means that the ts-**2a**-o-ene is 27.4 kcal/mol relative to *trans*-**2a**-oxo, which makes it more unlikely that it is the major reaction path at room temperature. The reaction between *trans*-**2a**-oxo and styrene generates *trans*-**2a**-o-ene (triplet) by overcoming a free energy barrier of 22.8 kcal/mol via ts-*trans*-**2a**-o-ene, which is the lowest barrier located for this step and also a reasonable activation energy at ambient conditions. A further oxygen−carbon bond formation that leads to *trans*-**2a**-epo-ene (singlet) proceeds via a spin-crossing transformation (Figure S19). A minimum energy crossing point (MECP) was located on the hypersurface where the two spin states have the same energy.[45−48] A calculated transition free energy barrier between two spin states is only 5.2 kcal/mol.

The only geometrical difference between **2a**-oxo and *trans*-**2a**-oxo is the position of the dissociated carboxylate group, which is near the oxo in **2a**-oxo and far from the oxo in *trans*-**2a**-oxo. This geometrical difference makes the reactivity toward styrene slightly different. The free energy barrier reached 25.2 kcal/mol when **2a**-oxo reacted with styrene, and the free energy of product **2a**-o-ene is 7.0 kcal/mol higher than the reactants. In contrast, the free energy barrier for the reaction between *trans*-**2a**-oxo and styrene is at 22.8 kcal/mol (taking *trans*-**2a**-oxo as a reference), and the free energy of product *trans*-**2a**-*o*-ene is 3.0 kcal/mol higher than the reactants. A possible explanation of the difference in reactivity is based on the electron density at the oxo of Ru^{IV}═O along the reaction path.

Along the reaction coordinate between **2a**-oxo and styrene (Table 1), negative charge builds up on the oxygen atom (from −0.43 to −0.51, finally to −0.56). The repulsion between this

DOI: 10.1021/acscatal.5b00496
ACS Catal. 2015, 5, 3966−3972

Table 1. Atomic Charges from Mulliken Population Analysis of Reaction between 2a-oxo and Styrene

complexes	charge of O of oxo group
2a-oxo	−0.43
ts-**2a**-*o*-ene	−0.51
2a-*o*-ene	−0.56
trans-**2a**-oxo	−0.44
ts-*trans*-**2a**-*o*-ene	−0.50
trans-**2a**-*o*-ene	−0.55

oxygen and the dissociated carboxylate group (carrying a formal negative charge) nearby thereby increases, which may cause the slightly higher free energy of both ts-**2a**-*o*-ene and **2a**-*o*-ene. However, for *trans*-**2a**-oxo (Table 1), although negative charge still builds up along the reaction coordinates, the dissociated carboxylate group is far from the oxo, and the electronic repulsion is minimal for both ts-*trans*-**2a**-*o*-ene and *trans*-**2a**-*o*-ene. Although there may be additional explanations for the difference in reactivity, it appears that **2a**-oxo needs to be transformed to *trans*-**2a**-oxo before reacting with styrene and completing the epoxidation of styrene. On the basis of a suggestion from one of the reviewers, we calculated the reactivity of the two conformations but with the carboxylate removed. In that way, we could distinguish the effect of the carboxylate placement versus the cis/trans placement of the picolinate moiety. We found that also, here, the reactivity slightly favors the same conformation that we found more reactive, but the effect is smaller (Figure S24). This result indicates that the preference of reactivity at *trans*-**2a**-oxo over **2a**-oxo could be due to a combination of the placements of the ligands bound to the metal and the placement of the nonbonded carboxylate group.

On the basis of our results, the hemilabile carboxylate of the Ru-pdc alkene epoxidation catalysts is essential for the catalytic function. It has several functions along the H_2O_2-driven alkene epoxidation reactions: (1) The tridentate coordination of the pdc^{2-} ligand stabilizes the stating complex (in comparison with Ru catalysts with five-coordinated ligands) when substrates are not present or not accessible. (2) The hemilabile nature of the ligand allows for substrate coordination. Although the tridentate coordination stabilized the complex, it could potentially block reactivity. However, the pdc ligand can clearly create a free site with low activation barriers. (3) In the formation of the Ru^{IV}═O intermediate, the dissociated carboxylate is directly involved. In the first step, a proton is transferred from the coordinated H_2O_2 to the carboxylate, then the proton is transferred to the noncoordinated oxygen, leading to formation of water and Ru^{IV}═O. 4) The p-donating nature of the ligand facilitates the oxidation by stabilizing the high oxidation states of the ruthenium center via p(O)−d(Ru) orbital overlap and charge compensation.

CONCLUSION

A DMSO-substituted [Ru(pdc)(tpy)] complex **1**-DSMO has been isolated and characterized by ^{1}H NMR, elemental analysis, MS, and X-ray crystallography. The kinetics of the ligand substitution reaction has been studied and revealed an associative ligand exchange pathway. This finding led to understanding the process of H_2O_2 entering the coordination sphere of the Ru-pdc alkene epoxidation catalysts. The structure of **1**-DMSO inspired us to propose a Ru^{IV}═O species, *trans*-**2a**-oxo, that is likely the active species for alkene epoxidation. The large difference in activity between **2a**-oxo and *trans*-**2a**-oxo indicates the importance of the dissociated carboxylate group, which is near and far, respectively, from the reacting oxo group. The species with the dissociated carboxylate group close to the reacting oxo will experience electrostatic repulsion along the reaction and will therefore have a high free energy of activation. In contrast, the species with the dissociated carboxylate group far from the oxo avoids this repulsion, and the reaction can proceed with a low activation free energy. The hemilabile property of the pdc^{2-} ligand is key to the facile transformation from the reactant all the way to the product, and the ligand's tridentate coordination also stabilizes the complex toward degradation. Our discovery has improved the understanding of the epoxidation mechanism catalyzed by the [Ru(pdc)(N^N^N)] catalysts. The fact that the carboxylate ligands, such as pdc^{2-}, are hemilabile and readily rearrange could also have implications on other catalytic processes in which these ligands are involved; for instance, the water oxidation reaction catalyzed by catalysts $[Ru(pdc)(pic)_3]$ and $[Ru(hqc)(pic)_3]$ (pic = 4-picoline; H_2hqc = 8-hydroxyquinoline-2-caboxylic acid).

ASSOCIATED CONTENT

Supporting Information

The Supporting Information is available free of charge on the ACS Publications website at DOI: 10.1021/acscatal.5b00496.

Crystallographic data for $C_{24}H_{20}N_4O_5RuS$ (CIF)
Proton NMR spectra of complex **1**-DMSO, kinetic measurement data, and DFT calculation results (PDF)

AUTHOR INFORMATION

Corresponding Authors

*E-mail: lichengs@kth.se.
*E-mail: ahlqui@kth.se.

Present Address

[¶](Y.W.) Department of Chemical Engineering, Stanford University, Stanford, California 94305, United States, and SUNCAT Center for Interface Science and Catalysis, SLAC National Accelerator Laboratory, 2575 Sand Hill Road, Menlo Park, California 94025, United States.

Author Contributions

[□]Y.W. and L.D. contributed equally to this work.

Notes

The authors declare no competing financial interest.

ACKNOWLEDGMENTS

This work was financially supported by the Swedish Research Council (Vetenskapsrådet), the Swedish Energy Agency, the Knut and Alice Wallenberg Foundation, and the China Scholarship Council (CSC). Computational resources have been provided by the PDC supercomputer center at KTH.

REFERENCES

(1) Johnson, R. A.; Sharpless, K. B. In *Catalytic Aymmetric Synthesis*; Ojima, I., Ed.; VCH: New York, 1993; pp 103−158.
(2) Katsuki, T. *Adv. Synth. Catal.* **2002**, *344*, 131−147.
(3) Jacobsen, E. N. In *Catalytic Aymmetric Synthesis*; Ojima, I., Ed.; VCH: New York, 1993; pp 159−202.
(4) Arends, I. W. C. E. *Angew. Chem., Int. Ed.* **2006**, *45*, 6250−6252.
(5) Berkessel, A.; Kaiser, P.; Lex, J. *Chem. - Eur. J.* **2003**, *9*, 4746−4756.
(6) Gross, Z.; Ini, S. *Org. Lett.* **1999**, *1*, 2077−2080.

DOI: 10.1021/acscatal.5b00496
ACS Catal. 2015, 5, 3966−3972

(7) Kureshy, R. I.; Khan, N. H.; Abdi, S. H. R.; Iyer, P. *J. Mol. Catal. A: Chem.* **1997**, *124*, 91−97.
(8) Kureshy, R. I.; Khan, N. H.; Abdi, S. H. R.; Patel, S. T.; Iyer, P. *J. Mol. Catal. A: Chem.* **1999**, *150*, 163−173.
(9) Kureshy, R. I.; Khan, N. H.; Abdi, S. H. R.; Patel, S. T.; Iyer, P. *J. Mol. Catal. A: Chem.* **1999**, *150*, 175−183.
(10) Stoop, R. M.; Bachmann, S.; Valentini, M.; Mezzetti, A. *Organometallics* **2000**, *19*, 4117−4126.
(11) Chatterjee, D. *Coord. Chem. Rev.* **2008**, *252*, 176−198.
(12) M. Stoop, R. M.; Mezzetti, A. *Green Chem.* **1999**, *1*, 39−41.
(13) End, N.; Pfaltz, A. *Chem. Commun.* **1998**, 589−590.
(14) Stoop, R. M.; Bauer, C.; Setz, P.; Wörle, M.; Wong, T. Y. H.; Mezzetti, A. *Organometallics* **1999**, *18*, 5691−5700.
(15) Augier, C.; Malara, L.; Lazzeri, V.; Waegell, B. *Tetrahedron Lett.* **1995**, *36*, 8775−8778.
(16) Nakata, K.; Takeda, T.; Mihara, J.; Hamada, T.; Irie, R.; Katsuki, T. *Chem. - Eur. J.* **2001**, *7*, 3776−3782.
(17) Francàs, L.; González-Gil, R. M.; Moyano, D.; Benet-Buchholz, J.; García-Antón, J.; Escriche, L.; Llobet, A.; Sala, X. *Inorg. Chem.* **2014**, *53*, 10394−10402.
(18) Fackler, P.; Huber, S. M.; Bach, T. *J. Am. Chem. Soc.* **2012**, *134*, 12869−12878.
(19) Koya, S.; Nishioka, Y.; Mizoguchi, H.; Uchida, T.; Katsuki, T. *Angew. Chem., Int. Ed.* **2012**, *51*, 8243−8246 S8243/1-S8243/12 .
(20) Dakkach, M.; Atlamsani, A.; Parella, T.; Fontrodona, X.; Romero, I.; Rodriguez, M. *Inorg. Chem.* **2013**, *52*, 5077−5087.
(21) Di Giovanni, C.; Vaquer, L.; Sala, X.; Benet-Buchholz, J.; Llobet, A. *Inorg. Chem.* **2013**, *52*, 4335−4345.
(22) Moosavifar, M.; Tangestaninejad, S.; Moghadam, M.; Mirkhani, V.; Mohammadpoor-Baltork, I. *J. Mol. Catal. A: Chem.* **2013**, *377*, 92−101.
(23) Vaquer, L.; Riente, P.; Sala, X.; Jansat, S.; Benet-Buchholz, J.; Llobet, A.; Pericas, M. A. *Catal. Sci. Technol.* **2013**, *3*, 706−714.
(24) Di Giovanni, C.; Poater, A.; Benet-Buchholz, J.; Cavallo, L.; Sola, M.; Llobet, A. *Chem. - Eur. J.* **2014**, *20*, 3898−3902.
(25) Francas, L.; Gonzalez-Gil, R. M.; Moyano, D.; Benet-Buchholz, J.; Garcia-Anton, J.; Escriche, L.; Llobet, A.; Sala, X. *Inorg. Chem.* **2014**, *53*, 10394−10402.
(26) Hazari, A. S.; Das, A.; Ray, R.; Agarwala, H.; Maji, S.; Mobin, S. M.; Lahiri, G. K. *Inorg. Chem.* **2015**, *54*, 4998−5012.
(27) Nishiyama, H.; Shimada, T.; Itoh, H.; Sugiyama, H.; Motoyama, Y. *Chem. Commun.* **1997**, 1863−1864.
(28) Tse, M. K.; Döbler, C.; Bhor, S.; Klawonn, M.; Mägerlein, W.; Hugl, H.; Beller, M. *Angew. Chem., Int. Ed.* **2004**, *43*, 5255−5260.
(29) Tse, M. K.; Bhor, S.; Klawonn, M.; Anilkumar, G.; Jiao, H.; Spannenberg, A.; Döbler, C.; Mägerlein, W.; Hugl, H.; Beller, M. *Chem. - Eur. J.* **2006**, *12*, 1875−1888.
(30) Bhor, S.; Anilkumar, G.; Tse, M. K.; Klawonn, M.; Döbler, C.; Bitterlich, B.; Grotevendt, A.; Beller, M. *Org. Lett.* **2005**, *7*, 3393−3396.
(31) Tse, M. K.; Klawonn, M.; Bhor, S.; Döbler, C.; Anilkumar, G.; Hugl, H.; Mägerlein, W.; Beller, M. *Org. Lett.* **2005**, *7*, 987−990.
(32) Anilkumar, G.; Bhor, S.; Tse, M. K.; Klawonn, M.; Bitterlich, B.; Beller, M. *Tetrahedron: Asymmetry* **2005**, *16*, 3536−3561.
(33) An, J.; Duan, L.; Sun, L. *Faraday Discuss.* **2012**, *155*, 267−275.
(34) Duan, L.; Xu, Y.; Gorlov, M.; Tong, L.; Andersson, S.; Sun, L. *Chem. - Eur. J.* **2010**, *16*, 4659−4668.
(35) Tong, L.; Wang, Y.; Duan, L.; Xu, Y.; Cheng, X.; Fischer, A.; Ahlquist, M. S. G.; Sun, L. *Inorg. Chem.* **2012**, *51*, 3388−3398.
(36) Couchman, S. M.; Dominguez-Vera, J. M.; Jeffery, J. C.; McKee, C. A.; Nevitt, S.; Pohlman, M.; White, C. M.; Ward, M. D. *Polyhedron* **1998**, *17*, 3541−3550.
(37) Technol., A. *CrysAlis Sofware System*, 171.36.32 ed.; Agilent Technologies: Santa Clara, CA, 2013.
(38) Sheldrick, G. M. *Acta Crystallogr., Sect. A: Found. Crystallogr.* **2008**, *64*, 112−122.
(39) Sheldrick, G. M. *SHELXL97; Program for Solution of Crystal Structure*; University of Gottingen: Gottingen, Germany, 1997.
(40) Becke, A. D. *J. Chem. Phys.* **1993**, *98*, 5648−5652.
(41) Lee, C.; Yang, W.; Parr, R. G. *Phys. Rev. B: Condens. Matter Mater. Phys.* **1988**, *37*, 785−789.
(42) Zhao, Y.; Truhlar, D. G. *Theor. Chem. Acc.* **2008**, *120*, 215−241.
(43) Martin, J. M. L.; Sundermann, A. *J. Chem. Phys.* **2001**, *114*, 3408−3420.
(44) Marten, B.; Kim, K.; Cortis, C.; Friesner, R. A.; Murphy, R. B.; Ringnalda, M. N.; Sitkoff, D.; Honig, B. *J. Phys. Chem.* **1996**, *100*, 11775−11788.
(45) Bearpark, M. J.; Robb, M. A.; Bernhard Schlegel, H. *Chem. Phys. Lett.* **1994**, *223*, 269−274.
(46) Koga, N.; Morokuma, K. *Chem. Phys. Lett.* **1985**, *119*, 371−374.
(47) Lundberg, M.; Siegbahn, P. E. M. *Chem. Phys. Lett.* **2005**, *401*, 347−351.
(48) Harvey, J. N.; Aschi, M.; Schwarz, H.; Koch, W. *Theor. Chem. Acc.* **1998**, *99*, 95−99.

DOI: 10.1021/acscatal.5b00496
ACS Catal. 2015, 5, 3966−3972